The International Journal of Advanced Manufacturing Technology (2019) 102:443–455
https://doi.org/10.1007/s00170-018-3093-4

ORIGINAL ARTICLE

Investigation on the effect of mandrels on hollow shafts in cross-wedge rolling

Xu Huang [1,2] · Baoyu Wang [1,2] · Yanhong Mu [1,2] · Jinxia Shen [1,2] · Junling Li [1,2] · Jing Zhou [1,2]

Received: 5 July 2018 / Accepted: 20 November 2018 / Published online: 4 January 2019

Abstract
Cross-wedge rolling (CWR) hollow shafts with mandrels can control the hole contour and reduce internal defects so that the working conditions for the shafts can be met. The diameter of the mandrel plays an important role in this forming process. In this study, numerical simulations and experimental trials were conducted as part of a detailed investigation on the mechanism of a mandrel and its influence on the forming quality of CWR hollow shafts. The contact areas between the mandrel and workpiece, the rolling forces of the mandrel, stress-strain fields, metal flows and temperatures were analysed in detail. The gaps on the surface of dies designed to prevent torsion failure of the rolled piece lead to noticeable steps on the surface of the rolled piece, as the relative diameter of the mandrel is too large. The diameter and non-circularity of the outer and inner surface increase with the increase of the relative diameter of the mandrel. The results can provide theoretical guidance for the production application of cross-wedge rolling hollow shafts with mandrels.

Keywords Cross-wedge rolling · Hollow shafts · Mechanism of mandrel · Forming quality

1 Introduction

Cross-wedge rolling (CWR) is a near-net-shape forming process, capable of reducing costs and improving the quality of the axis and shaft parts [1]. With the increasing demand for lightweight construction in the automotive industry, hollow shafts are needed in large numbers. The polar moment of inertia and the section modulus in torsion of a hollow shaft is greater than that of a solid shaft under the same amount of material. The material of a hollow shaft is more widely distributed in high-stress areas that can make full use of the materials. The major plastic processing methods of a hollow shaft are radial forging [2, 3], extrusion [4, 5], and rotary compression [6, 7]. The CWR process is a new forming technique for the production of hollow shafts that reduces costs while improving the quality.

There have been several theoretical and experimental studies on the production of hollow shafts by CWR. Zhang et al. [8, 9] studied the wall thickness of hollow shafts rolled using cross-wedge rolling using rolling experiments and presented the impact rules of the main factors on the wall thickness of a hollow workpiece. Wang et al. [10] simulated the sizing process of CWR in various conditions and revealed the relationship between the wall thickness of hollow parts and the strain and stress fields. Pater et al. [11–13] explored the influence of process parameters on the forming process stability using a three-roll cross-wedge rolling method and analysed the dependences between process stability, deformation ratio and wall thickness of the material formed by flat cross-wedge rolling. Urankar et al. [14, 15] investigated the limits of forming hollow products with CWR via experiments and the explicit finite-element method. By varying the billet wall thickness and material, area reduction, and tool geometry, a dimensionless crushing parameter was introduced for predicting operating conditions that lead to part failure. Furthermore, a criterion was developed for the crushing of hollow billets in the CWR process. An analytical model was developed for determining the critical friction condition in the cross-wedge rolling of hollow shafts. Peng et al. [16] derived the deflection angle

✉ Baoyu Wang
bywang@ustb.edu.cn

[1] School of Mechanical Engineering, University of Science and Technology Beijing, No. 30 Xueyuan Road, Haidian District, Beijing 100083, China

[2] Beijing Key Laboratory of Metal Lightweight Forming and Manufacturing, Beijing, China

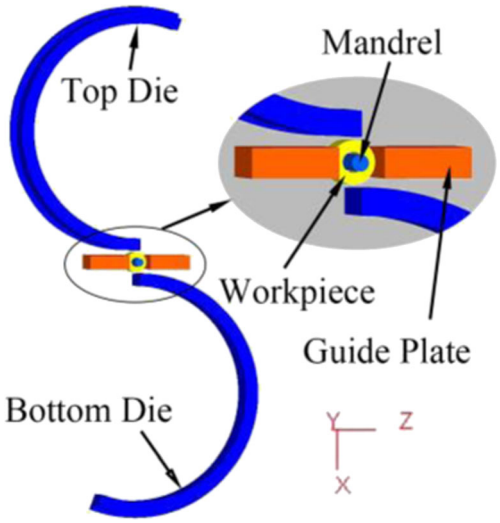

Fig. 1 FEM model of cross-wedge rolling

equations of side-wedges applied at the multi-wedge cross-wedge rolling of hollow shafts and verified the feasibility of producing large and long thick-walled hollow shafts with double-wedge CWR. Ji et al. [17–19] analysed the mechanism of material flow, the temperature distribution and the strain and rolling force in CWR for a hollow engine valve without a mandrel, explored the influence of various process parameters on ovality and the inner diameter of the hollow valve billet, and significantly improved the inner hole reaming phenomenon at both sides of the wedge position by way of the variable stretching angle design of the die.

The aforementioned studies on hollow parts were performed on cross-wedge rolling hollow shafts without mandrels. However, the hole contour of the cross-wedge rolling hollow shaft without a mandrel was formed in an uncontrolled manner because the material was able to freely flow into the hollow. Cross-wedge rolling hollow shafts with a mandrel can control the inner contour and improve the internal defects to meet the working conditions for the shafts. However, it has rarely been applied to the production of hollow shafts because of insufficient theoretical and technical knowledge of the effect of a mandrel on the forming quality of a rolled piece. Yang et al. [20] assembled a middle support roller into a shaft middle hole during 3-roller CWR to achieve internal and external precision forming for a hollow motor shaft. Landgrebe et al. [21] presented a modified CWR process, which enables the manufacturing of hollow shafts from solid cylindrical billets in which the actively driven mandrels pierce axially into the workpiece. Neugebauer et al. [22–24] proposed two approaches of applying a stationary mandrel or the relative motion of moving mandrels to form the inner contour of the hollow shafts by CWR, and analysed the effect of a rolling parameter on rolling force and rolling limit for hollow parts. Jiang et.al. [25] investigated the process of cross-wedge rolling for

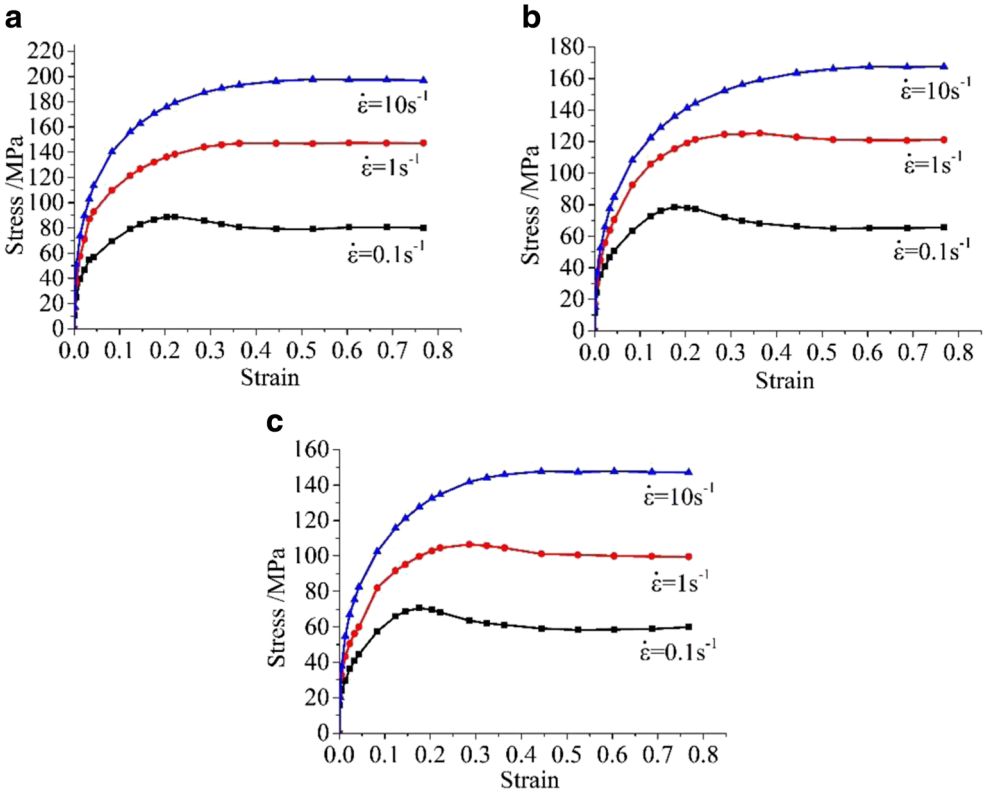

Fig. 2 Stress-strain curves of 40 MnBH. **a** T = 950 °C. **b** T = 1000 °C. **c** T = 1050 °C

Table 1 Parameters of cross-wedge rolling simulation

Parameter	Value
Speed of roll (rpm)	10
Workpiece temperature (°C)	1000
Tools temperature (°C)	20
Environment temperature (°C)	20
Contact heat transfer coefficient ($W/m^2 \cdot K$)	40×10^3
Convection coefficient ($W/m^2 \cdot K$)	20
Emissivity ($W/m^2 \cdot K$)	700
Friction factor between workpiece and die	1
Friction factor between workpiece and mandrel	0.3
Mesh number for billet	100,000
Billet material	40 MnBH
Outer diameter of billet (mm)	Φ50
Inner diameter of billet (mm)	Φ24
The forming angle (°)	38
The stretching angle (°)	4

manufacturing thick-walled hollow axles and determined the influence rules of forming angle, stretching angle, processing temperature and area reduction on the non-circularity of a rolled piece. Peng et al. [26, 27] proposed a laminated shaft production forming method involving cross-wedge rolling. The deformation characteristics of the laminated shafts were obtained and the formation mechanisms of the stress distributions were analysed. Ji et al. [28] applied the method of combined CWR and forging process to the production of a hollow valve and analysed the distributions of effective strain, force, torque, metal flow and temperature. Yang et al. [29, 30] investigated the relationships between the process parameters and ovality by analysing the influence of the helical and circular contact area between the roller and workpiece on the metal flow using the finite-element method, established a method for predicting the ovality of rolled piece and developed the process of cross-wedge rolling axle sleeves proximately without a stub bar.

There is no doubt that mandrel diameter plays an important role in the CWR process with a mandrel. However, this factor has been neglected in previous studies. In this study, numerical simulation and experimental trials were conducted to investigate the mechanism of a mandrel. The contact areas between the mandrel and workpiece, the rolling forces of the mandrel, stress-strain fields, metal flows and temperatures were analysed in detail, and the influence of mandrels on the forming quality of the inner and outer surface of the rolled pieces was also discussed.

2 Numerical modelling of the cross-wedge rolling process

Given the mirror symmetry of the selected geometry and dies, only one half of the workpiece is considered by applying a constraint at the symmetry plane to reduce CPU processing time. The simplified geometric finite-element model of a cross-wedge rolling hollow shaft is shown in Fig. 1. The finite-element model was built based on the following assumptions: (1) The dies, guide plates and mandrel were considered to be rigid owing to their negligible elastic deformation. The workpiece was defined as a deformable body because of the large deformation and the ignorable elastic deformation. (2) The roller speed was set as a rotation velocity of 10 rpm in the numerical simulation to replicate the actual condition of the H630 rolling mill. (3) The material of the workpiece, 40 MnBH, was assumed to be isotropic and the yielding behaviour followed the von Mises yield criterion. The stress-strain curves, shown in Fig. 2, were measured by hot compression tests in a Gleeble-1500D mechanical simulator. (4) The contact between dies and workpiece was described using a shear friction model, which is used mostly for bulk-forming simulations. The friction coefficient between workpiece and mandrel was described similarly by shear friction model [31]. The friction between the

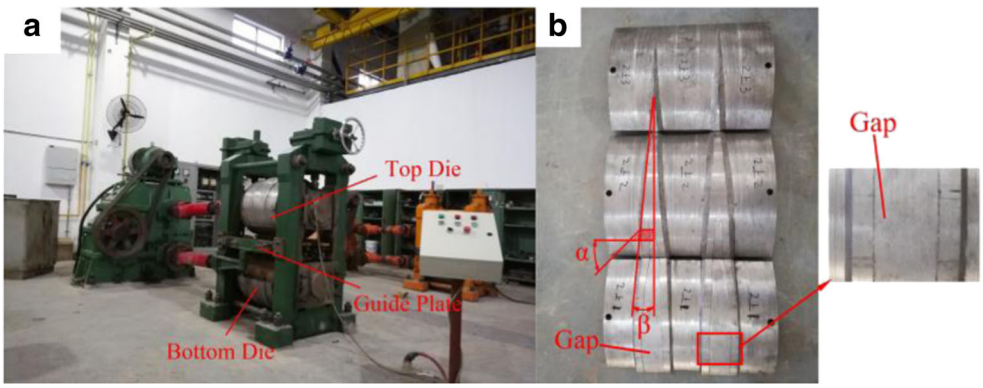

Fig. 3 Experimental equipment. **a** H630 mill. **b** Forming wedge tools, α = 38°, β = 4°

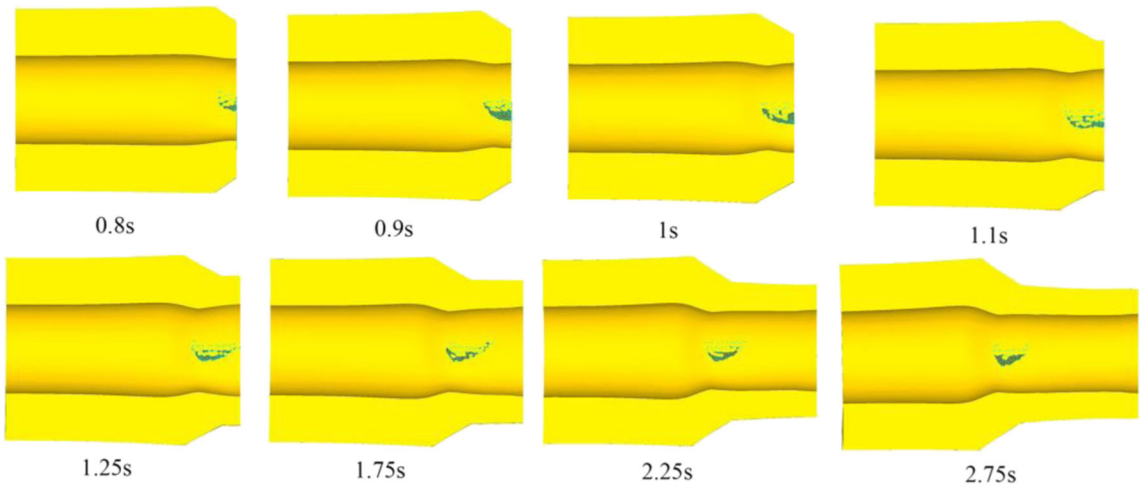

Fig. 4 Contact areas between mandrel and workpiece at various times ($i = 0.8$)

workpiece and guiding plate was neglected. The detailed parameters of the FE simulation are listed in Table 1.

3 CWR experiments

The experimental trials on the CWR process were conducted using the H630 mill as shown in Fig. 3a. The forming wedge tools are shown in Fig. 3b. In this study, the used hot rolled bar of 40 MnBH was produced by the Baosteel Corporation. To investigate the mechanism of a mandrel on CWR process, the relative diameter of the mandrel is defined by:

$$i = \frac{d}{D} \tag{1}$$

where d is the diameter of the mandrel and D is the inner diameter of billets. Five different relative diameters of the mandrel were selected: 0.6, 0.7, 0.8, 0.9 and 0.98. The billets were heated up to 1000 °C and soaked for 30 min in an electric tube furnace, then quickly transferred to the H630 rolling mill to be rolled. The temperature of the rolled piece was recorded using infrared thermography. The quality of the rolled part, including the surface quality and internal quality, was checked after water cooling.

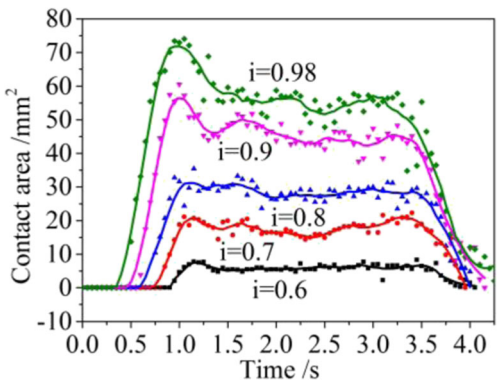

Fig. 5 Changes of contact area between mandrel and workpiece with time at different relative diameters of the mandrel

4 Results and discussion

4.1 Contact areas between workpiece and mandrel

The contact areas between the workpiece and mandrel reflect the range of the effect of the mandrel. Figure 4 shows the contact areas between the mandrel and workpiece at different times. At the beginning of rolling, the contact areas increase with time. Then, the contact areas remain stable after increasing to a certain value. The contact surface appears to be semicircular. Figure 5 shows the changes of the contact area between the mandrel and workpiece with time at different relative diameters of the mandrel. The contact area increases with the increase of the relative diameter of the mandrel. The value of contact area increases first and then decreases slightly to a stable value. The value of the radius reduction in the half circle is an important indicator to demonstrate the slight decrease of the contact area. Generally, the reduction in the half circle h is determined by the forming angle and stretching angle:

$$h = \pi r_k \tan\alpha \tan\beta \tag{2}$$

where r_k is the rolling radius of workpiece, α is the forming angle and β is the stretching angle. Compared with the stretching stage, the rolling radius of the workpiece in the knifing stage is larger. The larger reduction in the half circle caused by the larger rolling radius leads to significant metal circumferential flow and insufficient metal axial flow, and a larger contact area appears between the mandrel and the workpiece.

To effectively analyse the change of the contact area, contact lengths in circumferential and axial direction were measured (as shown in Fig. 6a). Figure 6b shows the time history of the contact lengths during the cross-wedge

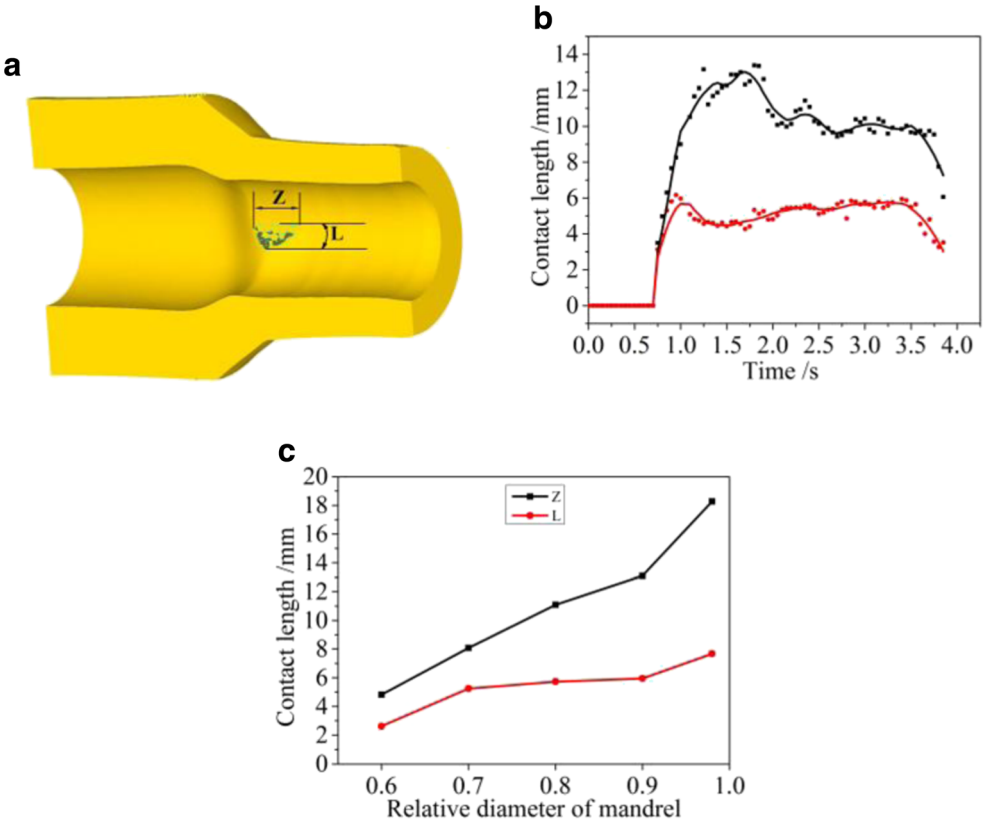

Fig. 6 Contact lengths between workpiece and mandrel. **a** Contact lengths measured. **b** Time history of contact lengths during cross-wedge rolling process (i = 0.8). **c** Contact lengths at different relative diameters of mandrel at 2.4 s

rolling process. It can be seen that the time histories of contact lengths are nearly identical qualitatively to the time history of the contact area. However, the contact length in the axial direction is almost twice that in the circumferential direction. Figure 6c shows the contact lengths at different relative diameters of the mandrel at 2.4 s. With the increase of relative diameter, the contact length in the axial direction increases much faster than that in the circumferential direction. During the process of cross-wedge rolling of hollow shafts, changing the relative diameter of the mandrel may lead to a change of contact area. The influence of relative diameter on the contact length in the axial direction is greater than that in the circumferential direction.

4.2 Reaction force of the mandrel

The effect of the mandrel on the forming quality of the workpiece during cross-wedge rolling is achieved by reaction force. Figure 7 presents the distribution of the reaction forces of the mandrel on the workpiece during the CWR process. According to the data in Fig. 7a, the time history of the axial force of the mandrel is nearly identical qualitatively. The axial forces increase rapidly when the inner hole of the billets comes into contact with the mandrel, then drop quickly to a stable value as the rolling process enters the stretch stage. According to the time history of the radial force of the mandrel shown in Fig. 7b, the radial forces of the mandrel on the workpiece

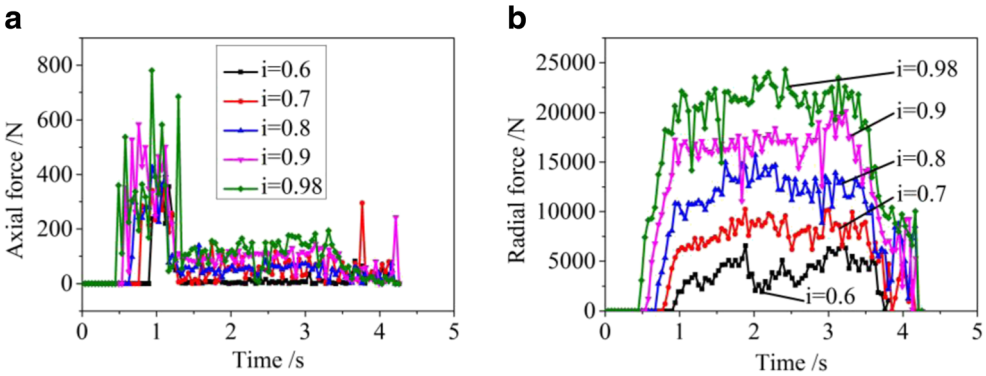

Fig. 7 Distribution of the reaction forces of mandrel on workpiece. **a** Axial forces of mandrel. **b** Radial forces of mandrel

increase rapidly at the beginning of the rolling process and remain stable until the end of the rolling process. Both the axial force and the radial force increase with the increase of the relative diameter. However, the maximum value of the axial forces is lower than 800 N, whereas the maximum value of the radial force is more than 5000 N and even exceeds 20,000 N when the relative diameter of the mandrel is 0.98. The axial forces are much smaller than the radial forces. Thus, it can be inferred that the main effect factor of the mandrel on the workpiece is radial force.

4.3 Stress and strain fields analysis

Figure 8 presents the stress field in the stretching zone at 1.5 s. The radial stress, circumferential stress and axial stress of the contact area between the mandrel and workpiece are compressive. The region of the radial compressive stress of the contact area increases when the relative diameter of the mandrel increases. When the relative diameter exceeds 0.8, greater radial compressive stress permeates the entire deformation zone. The circumferential stress near to the contact area is tensile stress when the relative diameter of the mandrel is 0.6. With

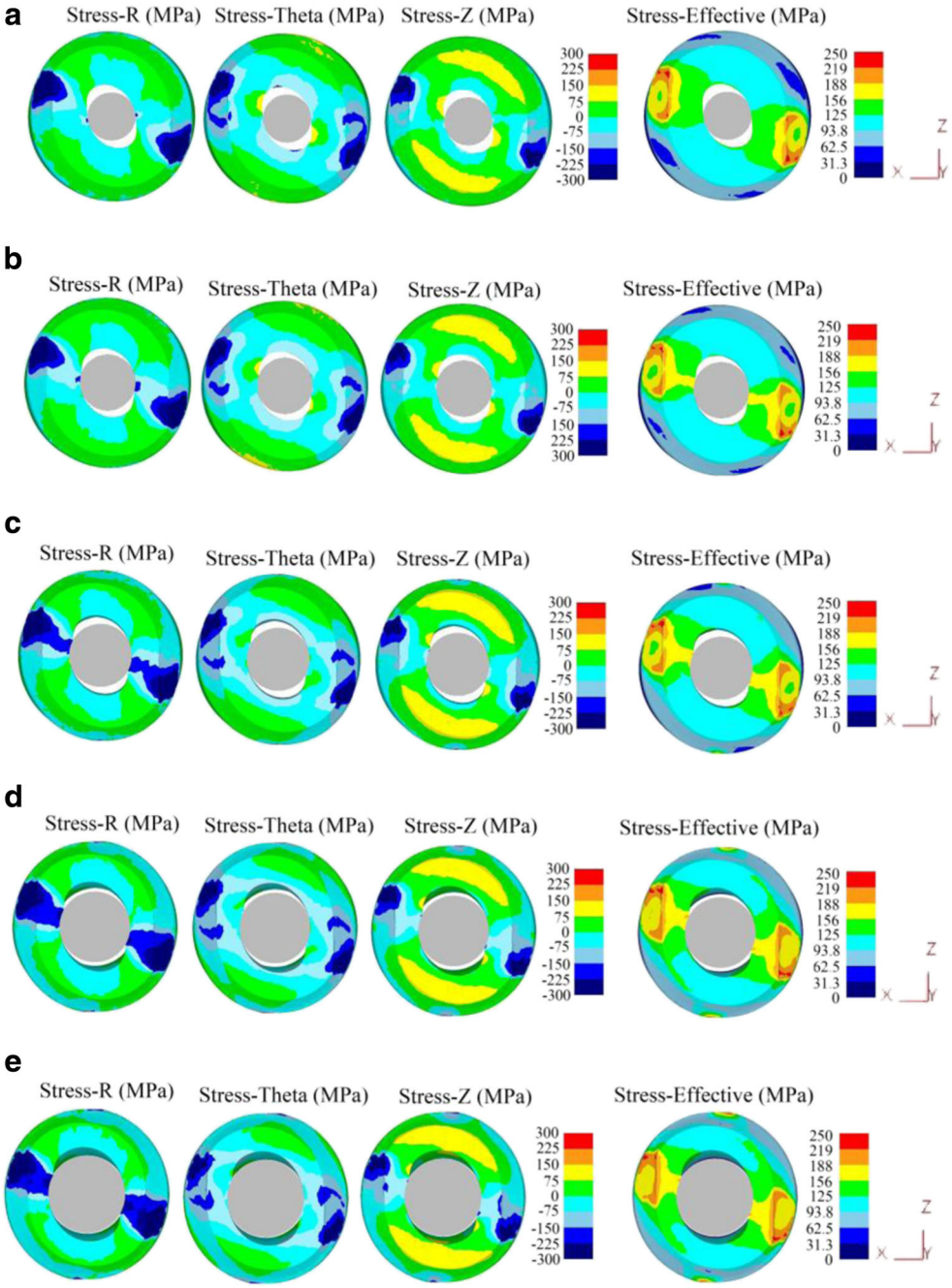

Fig. 8 Stress field distribution in the stretching zone. **a** $i = 0.6$. **b** $i = 0.7$. **c** $i = 0.8$. **d** $i = 0.9$. **e** $i = 0.98$

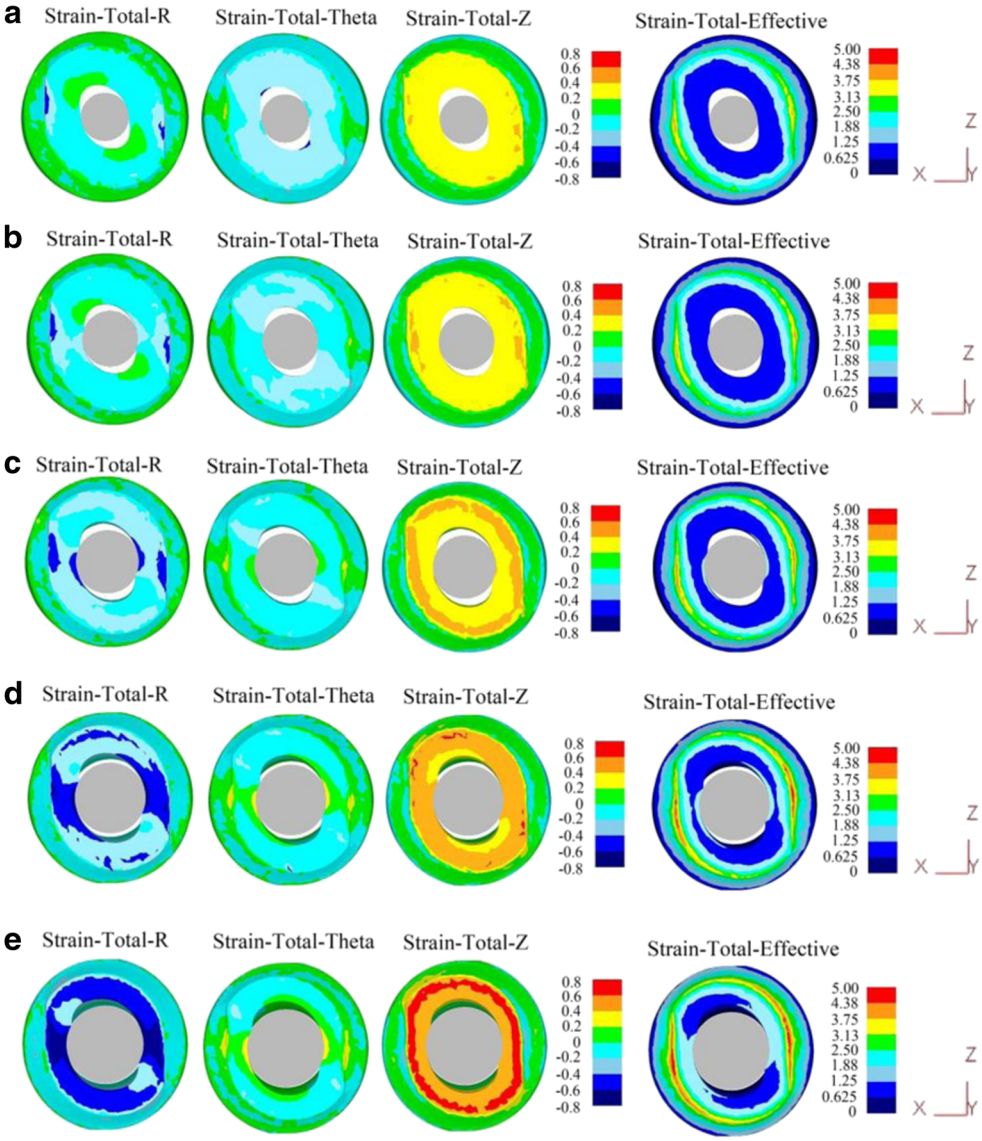

Fig. 9 Strain field distribution in the stretching zone. **a** $i = 0.6$. **b** $i = 0.7$. **c** $i = 0.8$. **d** $i = 0.9$. **e** $i = 0.98$

the increase of the relative diameter, the tensile stress decreases gradually. This can be attributed to the increased circumferential flow of metal caused by greater radial compression. The axial tensile stress outside the deformation zone spreads over the inner surface with the relative diameter of the mandrel ranging from 0.6 to 0.98. The effective stress of the deformation zone increases when the relative diameter of the mandrel increases.

Figure 9 presents the strain field in the stretching zone at 1.5 s. The radial strain of the contact area between the mandrel and workpiece is compressive. The circumferential strain and axial strain are tensile. The radial compressive strain, circumferential tensile strain and axial tensile strain of the contact area increase with the increase of the relative diameter of the mandrel. Meanwhile, the axial strain is more heterogeneous when the relative diameter of the mandrel is 0.98. The axial tensile strains of the inner and outer surfaces are significantly lower than that in the middle area. With the increase of relative diameter of the mandrel, the effect of the mandrel is intensified, and the greater radial compressive strain results in greater metal flow along the circumferential and axial direction. The effective strain shows that the strain on the outside surface is higher than that on the inner surface. The larger relative diameter of the mandrel leads to an increase of the effective strain on the inner surface.

4.4 Material flow analysis

Material flow has considerable influence on the forming quality of the rolled piece. Figure 10a shows the initial lateral grid. Figure 10b shows the lateral grid after deformation. The material shows considerable twisting in the rotational direction. The twisting degree increases from the inner surface to the outer surface of the rolled piece. Figure 10c shows the initial longitudinal single grid, and Fig. 10d shows the single longitudinal grid after deformation. Parallel element mesh

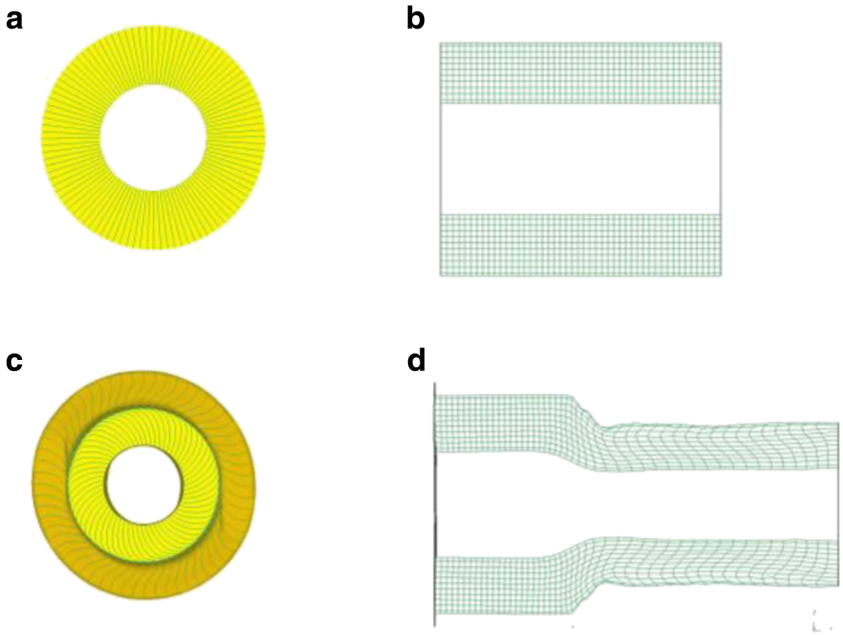

Fig. 10 Deformation grid during the CWR process ($i = 0.8$). **a** Initial lateral grid. **b** Lateral grid after deformation. **c** Initial longitudinal single-layer grid. **d** Longitudinal single-layer grid after deformation

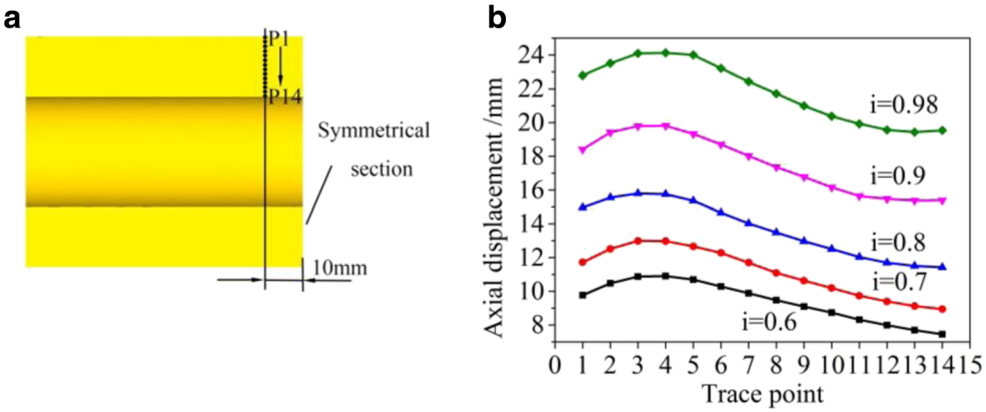

Fig. 11 The axial displacement in the CWR process. **a** The location of the tracing points. **b** The axial displacement of the tracing points after rolling

deformation also occurs. The axial flow of the material increases first and then decreases from the inner surface to the outer surface, and the difference increases as the rolling length increases. Axial uneven deformation is significant in the cross-wedge rolling process of hollow shafts with mandrels.

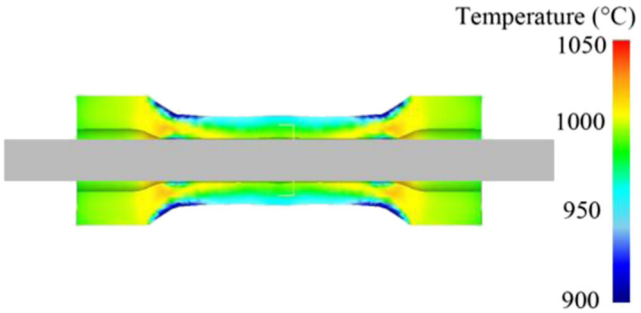

Fig. 12 Temperature distribution of the workpiece in the stretching zone

Inhomogeneous deformation is mainly attributed to the surface friction of the inner wall and outer wall.

To analyse the influence of the relative diameter of the mandrel on the metal flow, fourteen points (the sequence of which is from the outer surface towards the inner surface) on the section 10 mm from the symmetrical cross section were selected (Fig. 11a). Figure 11b shows the point in the axial displacement after rolling. The axial flow of metal varies as the relative diameter of the mandrel changes. As the relative diameter of the mandrel increases, the axial displacement of the entire cross-section increases, and the inhomogeneous flow of metal increases as well.

4.5 Temperature field analysis

Figure 12 presents the temperature distribution of the workpiece in the stretching zone. The result shows that the

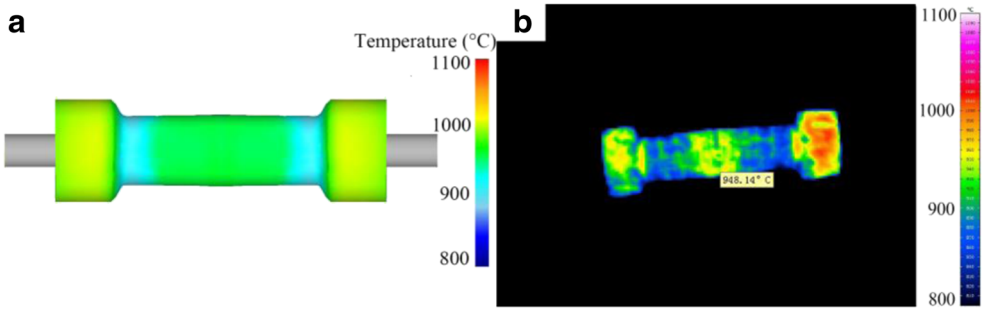

Fig. 13 Temperature distribution of rolled piece on the outside surface ($i = 0.8$). **a** FEM results. **b** Photograph recorded using infrared thermography

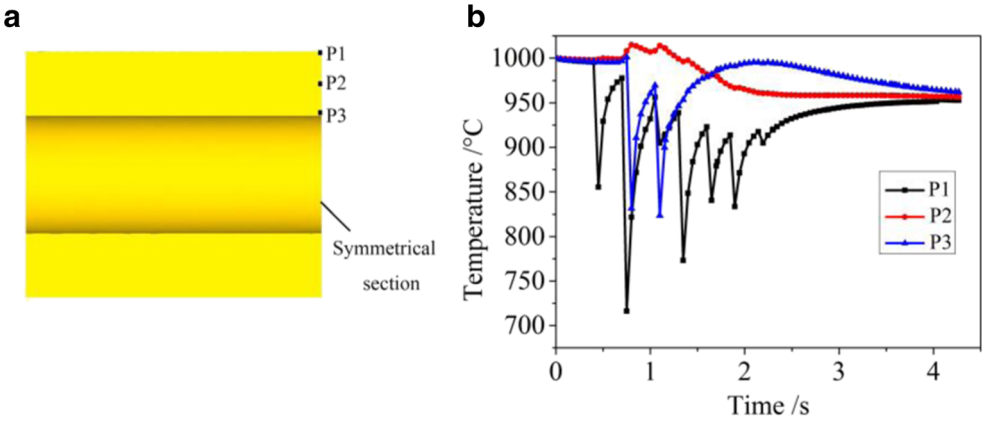

Fig. 14 Temperature distribution during the CWR process of hollow shaft. **a** The location of the tracing points. **b** The temperature of the tracing points during CWR process ($i = 0.8$)

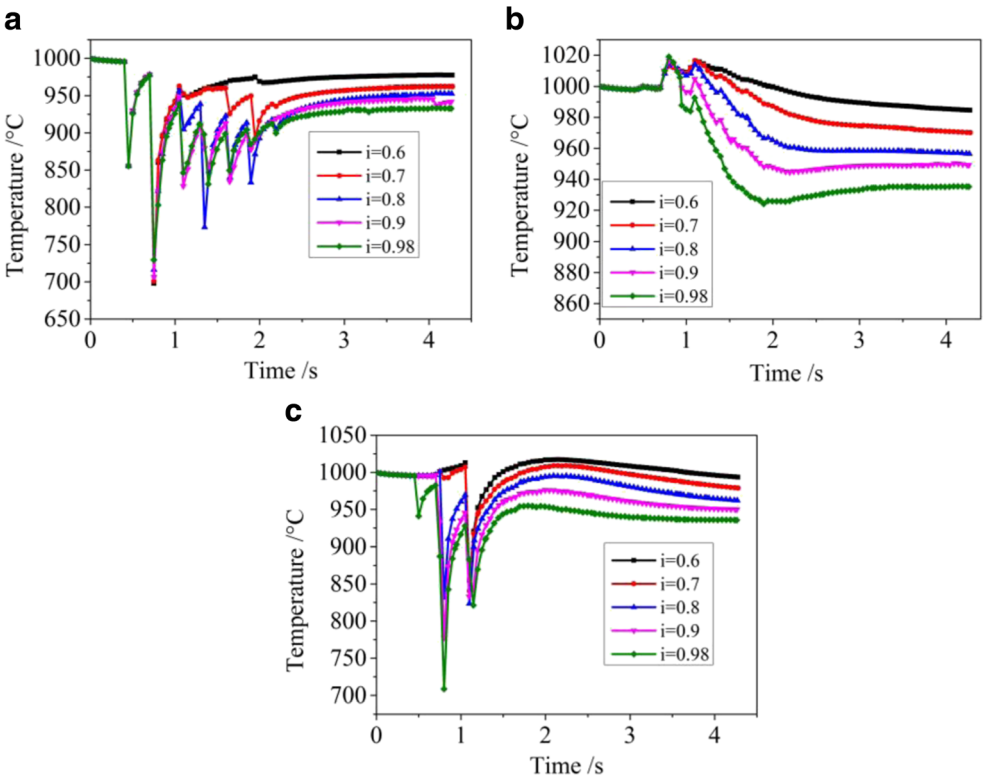

Fig. 15 Temperature distribution during the CWR process of hollow shaft. **a** P1. **b** P2. **c** P3

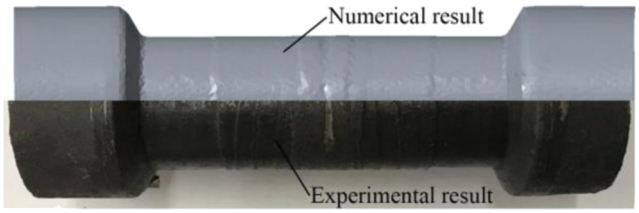

Fig. 16 Comparison of outer surface quality of the experimental and numerical results ($i = 0.8$)

temperature field is poorly homogeneous under the effect of heat exchange with air, dies and mandrel. The low-temperature regions are located mainly in the contact areas between the workpiece and die, as well as the contact areas between the workpiece and mandrel. The temperature in the entire deformation area is lower than that in the other regions of the workpiece. Figure 13 presents the temperature distribution of the rolled piece on the outside surface as per FEM and experimental tests, in which the results have good consistency.

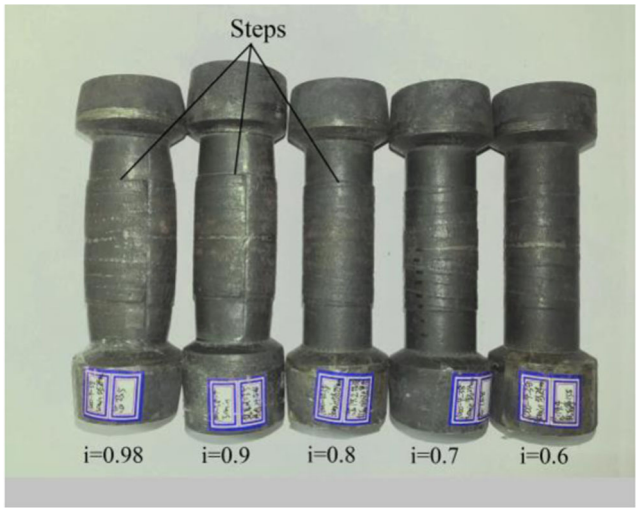

Fig. 17 Surface quality of the rolled piece for various relative diameters of the mandrel

During the CWR process, the temperature of the workpiece drops because of the heat exchange with the dies, the mandrel and the environment. Heat deformation causes the temperature to increase to a certain extent. To analyse the rolling temperature, three points (the sequence of which is from the outer surface towards the inner surface) on the symmetrical cross-section were selected for analysis. The locations of the points were presented in Fig. 14a. Figure 14b shows the time history of rolling temperature for three different tracking points. The trends of the time-temperature history vary widely. The temperatures of points 1 and 3 decrease rapidly and reach the minimum value when the points come into contact with the surfaces of the die and the mandrel. However, the temperature of point 2 increases with the process of rolling. The decrease of temperature at points 1 and 3 is mainly attributed to the heat exchange between the inner wall and outer wall, and the increase of temperature at point 2 can be ascribed to the heat deformation of metal. The temperature on the outside hole drops faster than the one on the inner surface owing to the larger contact area with die. The temperatures of points 1 and

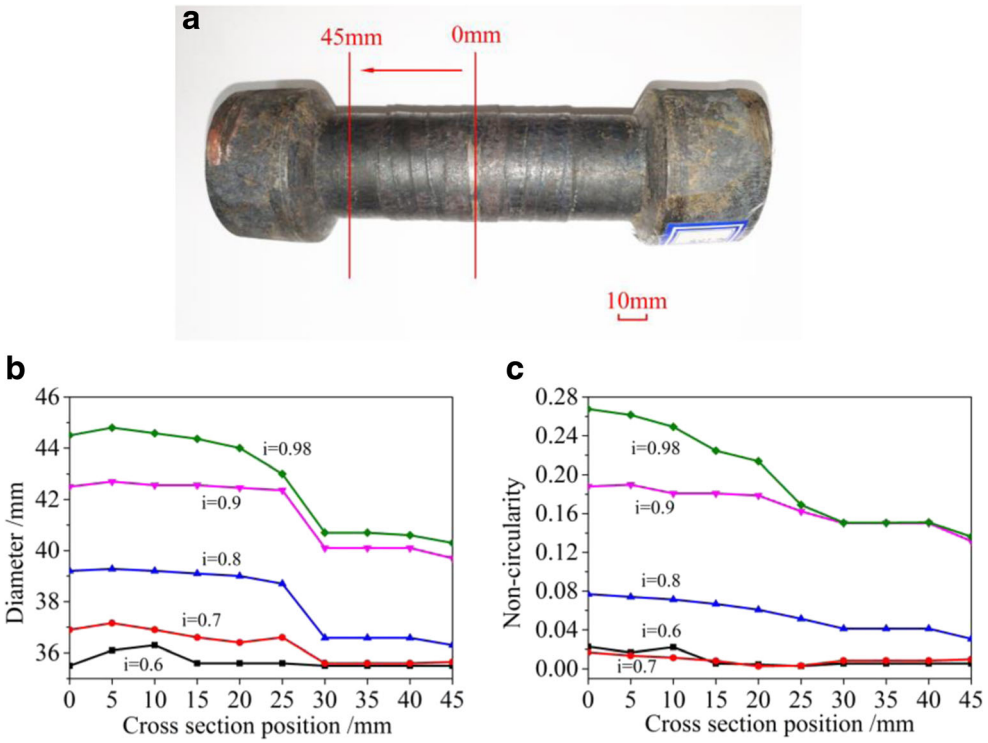

Fig. 18 Diameter and non-circularity of outer surface of the rolled piece. **a** The location of the sections. **b** The maximum diameter. **c** The non-circularity

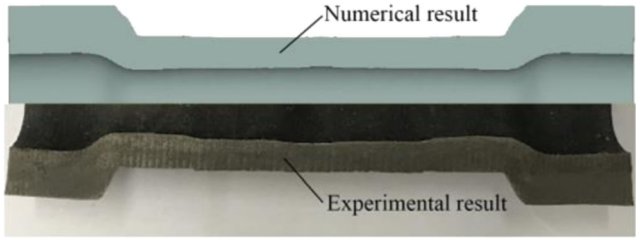

Fig. 19 Comparison of inner surface quality of the experimental and numerical results ($i = 0.8$)

3 rise in the later stages of the rolling process owing to the lack of surface contact and the heat exchange with the middle area, and the temperature of point 2 decreases because of the heat exchange with the inner and outer surfaces.

Figure 15 presents a comparison of the time history of rolling temperature during the CWR process when using different relative diameters of the mandrel. It can be seen that all temperatures of the three tracing points decrease with the increase of the relative diameter of the mandrel. Larger relative diameter results in larger contact area between the mandrel and billet, which leads to the increase of heat transmission. This can be verified by the large temperature drop of point 3 under larger relative diameter of the mandrel as shown in Fig. 15c. In addition, the wall thickness reduction of the rolled piece caused by larger relative diameter increases the temperature drop under the action of heat exchange with the environment.

4.6 Influence of mandrel on the surface quality of the rolled piece

The comparison of outer surface quality of the experimental and numerical results is shown in Fig. 16. The experimental and numerical results show high agreement. Obvious steps appear on the surfaces of the rolled pieces. Figure 17 shows the surface quality of the rolled piece rolled using different relative diameters of the mandrel. When the relative diameter of the mandrel is 0.6, the steps are not obvious. However, with the increase of relative diameter of the mandrel, the steps keep increasing. The defect can be attributed to the gaps on the surface of dies. To prevent torsion failure of the rolled piece, the gaps on the surface of dies were designed (as shown in Fig. 3b). This design is feasible when the relative diameter of the mandrel is small. However, with the increase of relative diameter of the mandrel, the large radial force of the mandrel on the workpiece leads to significant circumferential flow of metal and large ovality of cross-section during the CWR process. Repeated compression of tools caused by large ovality leads to metals flowing into the gap regions of dies.

To study the forming dimension of the rolled piece, an indicator for the non-circularity should be defined. The following formula was used to calculate the non-circularity:

$$e = \frac{2(D_{\max} - D_{\min})}{D_{\max} + D_{\min}} \tag{3}$$

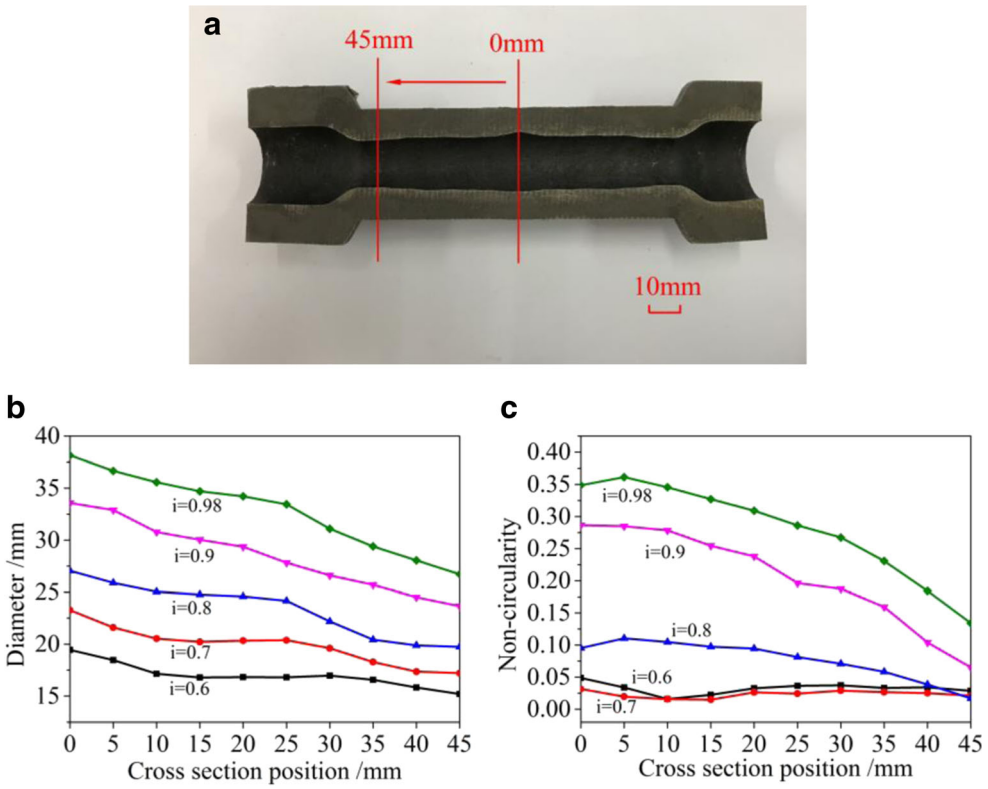

Fig. 20 Diameter and non-circularity of inner surface of the rolled piece. **a** The location of the sections. **b** The maximum diameter. **c** The non-circularity

where D_{max} is the largest diameter, D_{min} is the smallest diameter and e is the calculated non-circularity from the largest and smallest diameters of the rolled piece. Ten equally spaced cross-sections shown in Fig. 18a were selected in this study to analyse forming dimension. Figure 18b shows the maximum diameter of outer surface of the rolled piece. Figure 18c shows the non-circularity of outer surface of the rolled piece. The diameter and non-circularity of outer surface both increase with the increase of relative diameter of the mandrel. When the relative diameter is lower than 0.7, the maximum diameter of the outer surface is lower than 37 mm and the non-circularity is lower than 2.3%. And the dimensions of the formed parts are near the target diameter of 35 mm. However, when the relative diameter exceeds 0.9, both the diameter and non-circularity of outer surface increase rapidly. It is obvious that the rolled piece is squashed.

4.7 Influence of the mandrel on the inner diameter of the rolled piece

The comparison of inner surface quality of the experimental and numerical results is shown in Fig. 19. The experimental and numerical results show high agreement. To study the inner diameter, the rolled pieces were cut along the axial direction. Ten equally spaced cross-sections shown in Fig. 20a were selected in this study to analyse forming dimension. Figure 20b shows the maximum diameter of inner surface of the rolled piece. The inhomogeneity of the diameter along the axial direction increases with the increase of relative diameter of the mandrel. When the relative diameter is 0.6, the hole expansion area mainly focuses on the region 10 mm near the symmetrical cross-section. With the increase of the relative diameter, the length of the hole expansion region and the value of the hole expansion increase. When the relative diameter exceeds 0.9, the hole expansion extends throughout the entire inner hole. Figure 20c shows the non-circularity of inner surface of the rolled piece. The non-circularity of inner surface increases with the increase of relative diameter of the mandrel. When the relative diameter is lower than 0.7, the non-circularity is lower than 5%. However, when the relative diameter of the mandrel exceeds 0.9, the non-circularity of the inner surface increases rapidly.

5 Conclusions

Investigation on the mechanism and the influence of a mandrel on the forming quality of hollow shafts in cross-wedge rolling was performed via experiments and numerical analyses, leading to the following conclusions:

1. The contact area and rolling force between the mandrel and workpiece increases with increasing relative diameter of the mandrel. The maximum contact area appears at the end of the knifing stage. The influence of the relative diameter on the contact length in the axial direction is larger than that in the circumferential direction. Compared with the radial force of the mandrel, the axial force of the mandrel is negligibly small. The main effect factor of the mandrel on the workpiece is radial force.
2. A larger relative diameter of the mandrel leads to greater radial compressive stress and strain, and the axial displacement of the entire cross-section increases. The effective strain and stress permeate into the inner surface of the billet as the relative diameter increases. Axial inhomogeneous deformation is significant. The inhomogeneous deformation increases as the relative diameter increases.
3. The temperature of the billet decreases with the increase of the relative diameter of the mandrel. A larger relative diameter results in a greater contact area between the mandrel and billet, which accelerates the temperature drop of the inner hole. The wall thickness reduction of the rolled piece caused by a larger relative diameter increases the temperature drop under the action of heat exchange with the environment.
4. The gaps on the surface of the dies lead to noticeable steps on the surface of the rolled piece. With the increase of the relative diameter of the mandrel, the step defect becomes more obvious.
5. The diameter and non-circularity of the outer and inner surface increase with the increase of the relative diameter of the mandrel. The diameter and non-circularity increase slowly when the relative diameter is small. However, when the relative diameter exceeds 0.9, the diameter and non-circularity increase rapidly, and the rolled piece is squashed noticeably.

Funding information This work is supported by the Fundamental Research Funds for the Central Universities (Grant No. FRF-BD-17-003A). This work is also supported by the National Natural Science Foundation of China (Grant No. 51875036, Grant No.51705018).

References

1. Hu ZH, Zhang KS, Wang BY, Shu XD, Yang CP (2004) Forming technology and simulation of cross wedge rolling parts. Metall Ind Press, Beijing
2. Schmoeckel D, Speck FD (1995) Axial-radial forming of tubular components. CIRP Annals Manuf Tech 44(1):235–238
3. Chen J, Chandrashekhara K, Lekakh SN, Richards VL (2012) Study of void closure in hot radial forging process using 3d nonlinear finite element analysis. Int J Adv Manuf Tech 62(9–12):1001–1011
4. Li D, Yang H, Guo LG, Zeng WD, Zhang J (2015) Study on exit temperature evolution during extrusion for large-scale thick-walled

inconel 625 pipe by FE simulation. Int J Adv Manuf Tech 76(5–8): 1421–1435
5. Barbara R, Lorenzo D, Luca T (2016) Multi-goal optimization of industrial extrusion dies by means of meta-models. Int J Adv Manuf Tech:1–13
6. Pater Z, Gontarz A, Tomczak J, Bulzak T (2015) Producing hollow drive shafts by rotary compression. Arch Civ Mech Eng 15(4):917–924
7. Tomczak J, Pater Z, Bulzak T (2016) The influence of hollow billet thickness in rotary compression. Int J Adv Manuf Tech 82(5–8): 1281–1291
8. Zhang KS, Wang BY, Liu JP, Hu ZH (2000) Research on wall thickness of hollow workpiece rolled by cross wedge rolling. Forg Stam Technol 23(2):34–36
9. Zhang KS, Liu JP, Wang BY, Hu ZH (2001) Analysis on stable rolling condition of hollow workpiece rolled by cross wedge rolling. J Univ Sci Technol Beijing 23(2):155–157
10. Wang JL, Xu CG, Ren GS (2000) The numerical simulation on hollow part's precise sizing process with cross-wedge rolling. J Shanghai Jiaotong Univ (Science) 1:248–252
11. Bartnicki J, Pater Z (2005) Numerical simulation of three-rolls cross-wedge rolling of hollowed shaft. J Mater Process Tech 164(20):1154–1159
12. Bartnicki J, Pater Z (2004) The aspects of stability in cross-wedge rolling processes of hollowed shafts. J Mater Process Tech 155-156(1):1867–1873
13. Pater Z, Bartnicki J (2006) Wedge-rolls rolling of hollowed parts. J Ach Mater Manu Eng 18(1–2):407–410
14. Urankar S, Lovell M, Morrow C, Li Q, Kawada K (2006) Establishment of failure conditions for the cross-wedge rolling of hollow shafts. J Mater Process Tech 177(1–3):545–549
15. Urankar S, Lovell M, Morrow C, Li Q, Kawada K (2006) Development of a critical friction model for cross wedge rolling hollow shafts. J Mater Process Tech 177(1–3):539–544
16. Peng WF, Zheng SH, Chiu Y, Shu XD, Zhan LH (2016) Multi-wedge cross wedge rolling process of 42CrMo4 large and long hollow shaft. Rare Metal Mater Eng 45(4):836–842
17. Ji HC, Liu JP, Wang BY, Lin JG, Tang XF (2016) The process parameters effect of ovality in cross wedge rolling for hollow valve without mandril. MATEC Web Conf 80:13003
18. Ji HC, Liu JP, Wang BY, Tang XF, Huo YM, Zhou J, Hu ZH (2016) Constitutive relationship of 4Cr9Si2 and technological parameters on the inner bore of cross wedge rolling for preform hollow valves. Int J Adv Manuf Tech 86(9–12):1–13
19. Ji HC, Liu JP, Wang BY, Zheng ZH, Huang JH, Hu ZH (2015) Cross-wedge rolling of a 4Cr9Si2 hollow valve: explorative experiment and finite element simulation. Int J Adv Manuf Tech 77(1–4):15–26
20. YangYM CFW, Chen JC, Zhao J (2013) Study on load of hollow motor shaft by 4-roll cross wedge rolling. App Mech Mater 288: 267–270
21. Landgrebe D, Steger J, Böhmichen U, Bergmann M (2018) Modified cross-wedge rolling for creating hollow shafts. Procedia Manuf 21:53–59
22. Neugebauer R, Kolbe M, Glass R (2001) New warm forming processes to produce hollow shafts. J Mater Process Tech 119(1):277–282
23. Neugebauer R, Glass R, Kolbe M, Hoffmann M (2002) Optimisation of processing routes for cross rolling and spin extrusion. J Mater Process Tech 125(36):856–862
24. Neugebauer R, Glass R, Hoffmann M (2005) Spin extrusion-a new partial forming technology based on 7 nc-axes machining. CIRP Annals-Manuf Tech 54(1):241–244
25. Jiang Y, Wang BY, Hu ZH, Lin JG (2011) Numerical simulation for thick-walled hollow axle during cross wedge rolling. Adv Mater Research 337:270–273
26. Peng WF, Zhang JH, Huang GX, Liu WP, Shu XD, Zhu J (2016) Stress distributions during the cross-wedge rolling of composite 42CrMo/Q235 laminated shafts. Int J Adv Manuf Tech 83(1–4): 145–155
27. Wu ZJ, Peng WF, Shu XD (2017) Influence of rolling temperature on interface properties of the cross wedge rolling of 42CrMo/Q235 laminated shaft. Int J Adv Manuf Tech 91(1–4):517–526
28. Ji HC, Liu JP, Wang BY, Fu XB, Xiao WC, Hu ZH (2017) A new method for manufacturing hollow valves via cross wedge rolling and forging: numerical analysis and experiment validation. J Mater Process Tech 240:1–11
29. Yang CP, Hu ZH (2016) Research on the ovality of hollow shafts in cross wedge rolling with mandrel. Int J Adv Manuf Tech 83(1–4): 67–76
30. Yang CP, Ma JW, Hu ZH (2017) Analysis and design of cross wedge rolling hollow axle sleeve with mandrel. J Mater Process Tech 239:346–358
31. Fu XB, Wang BY, Zhu XX, Tang XF, Ji HC (2016) Numerical and experimental investigations on large-diameter gear rolling with local induction heating process. Int J Adv Manuf Tech 91(1–4):1–11